Electric field control of magnetic properties and electron transport in $BaTiO_3$-based multiferroic heterostructures

M. Asa[1], L. Baldrati[1], C. Rinaldi[1], S. Bertoli[1], G. Radaelli[1], M. Cantoni[1] and R. Bertacco[1]

[1] Dipartimento di Fisica, Politecnico di Milano, Via G. Colombo 81, 20133 Milano, Italy

E-mail: matteo.cantoni@polimi.it

Abstract. In this paper, we report on a purely electric mechanism for achieving the electric control of the interfacial spin polarization and magnetoresistance in multiferroic tunneling junctions. We investigate micrometric devices based on the Co/Fe/$BaTiO_3$/$La_{0.7}Sr_{0.3}MnO_3$ heterostructure, where Co/Fe and $La_{0.7}Sr_{0.3}MnO_3$ are the magnetic electrodes and $BaTiO_3$ acts both as ferroelectric element and tunneling barrier. We show that, at 20 K, devices with 2 nm thick $BaTiO_3$ barrier present both tunneling electro-resistance (TER=12±0.1%) and tunneling magneto-resistance (TMR). The latter depends on the direction of the $BaTiO_3$ polarization, displaying a sizable change of the TMR from -0.32±0.05% for the polarization pointing towards Fe, to -0.12±0.05% for the opposite direction. This is consistent with the on-off switching of the Fe magnetization at the Fe/$BaTiO_3$ interface, driven by the $BaTiO_3$ polarization, we have previously demonstrated in X-ray Magnetic Circular Dichroism experiments.

PACS: 72.25.Mk; 77.55.Nv; 77.55.fe; 77.80.bn; 77.84.Bw

1. Introduction

The search for room-temperature bulk multiferroic materials [1,2,3,4] and "artificial" multiferroic systems [5,6,7], i.e. systems separately displaying different ferroic orders coupled each other, currently generates strong theoretical and experimental efforts in condensed matter physics. This is crucial in view of the development of upcoming spintronic devices exploiting magnetoelectric coupling (MEC) to control the magnetic order acting on the ferroelectric one or *viceversa* [7,8,9]. For instance, multiferroics showing strong enough MEC could lead to spin-based devices with ultralow power consumption, thanks to the electrical writing of the magnetic information.

Electric writing, in particular, is a key issue in the development of Magnetic RAMs (MRAMs). A MRAM cell, in its basic configuration, is constituted by a magnetic tunneling junction (MTJ), where the magnetization of one electrode is fixed, while the other one (free layer) can be oriented in different directions. The resistance of the MTJ depends on the relative orientation of the two magnetizations (typically parallel or antiparallel), so that "writing" the cell means setting the second electrode magnetization in a given direction with respect to the first one. Despite many evident advantages of MRAMs (high access speed, non-volatility, endurance, radiation hardness) versus competing technologies (DRAMs, SRAMs, flashes), their spread is actually limited by the relatively large power consumption, due to the high current values needed for the writing process [10,11]. Among the viable approaches for solving this problem, such as Spin Transfer Torque (STT) [12,13,14], Spin Orbit Torque [15,16,17] and optical writing [18,19,20,21], the pure electric control of the magnetization is one of the most promising. The key idea is to employ a voltage pulse (with associated low current, and thus negligible energy dissipation) to modify by MEC some magnetic properties (coercive field, magnetization intensity, magnetization orientation, magnetic order) of the free layer.

However, single-phase multiferroics [1,2,3,4] often present low Curie temperatures and weak magnetoelectric coupling, thus hampering or limiting practical applications. Aiming at a large technological impact, multiferroic heterostructures, made of conventional ferromagnets (FM) and traditional ferroelectrics (FE), are more promising [5,6,7] .

In particular, hybrid magnetic-ferroelectric tunneling junctions (MFTJs) with a ferroelectric barrier, represent a very interesting architecture where both ferroelectric polarization and magnetization state can be used independently to store information. In this way up to four different states of resistance can be obtained thanks to the combination of tunneling magnetoresistance (TMR) and tunneling electroresistance (TER) [22,23,24,25,26,27,28,29,30].

As a matter of fact, interfacial MEC may determine a sizeable change of TMR for opposite states of ferroelectric polarization [24,25,27,31]. In case of half-doped manganite electrodes, the metal-to-insulator phase transition has been used to improve the TER by increasing the barrier thickness, eventually leading to the suppression of the interface ferromagnetism due to the strong link between ferromagnetism and metallicity [29,32]. This kind of engineered interfaces as well as new strategies for strain mediated magnetoelectric coupling [33] are promising routes to implement the electric control of magnetism in forthcoming devices.

Among many FM/FE heterostructures, Fe/$BaTiO_3$ has emerged as prototypical system. In fact Fe and $BaTiO_3$ (BTO) possess robust ferroic orders at room temperature and a negligible lattice mismatch (~1.6%) which favors epitaxial growth of Fe/BTO interfaces. Two kinds of ME coupling have been predicted at this interface: (i) direct coupling, owing to interfacial electronic effects, and (ii) indirect coupling, mediated by strain. The first one, leading to changes in the Fe surface magnetization and surface magnetocrystalline anisotropy, has been theoretically predicted and explained in terms of exchange-bias coupling at FM/FE interface [34,35,36,37], modulation of carrier density in FM layers [38,39], bond reconfiguration driven by ionic displacement at FM/FE interfaces [40] and spin dependent screening at FM/FE interfaces [41].

Experimentally it has been found that, for Fe thin films deposited on BTO single crystals, MEC is strain-mediated [42,43]. In Ref. 43 some of us demonstrated that the application of an electric field to the BTO substrate significantly alters the magnetic anisotropies and the coercivity of the Fe overlayer in epitaxial Fe/BTO(001) structures, leading to an increase of the coercive field by more than 100% in the

orthorhombic phase (250 K) and of the order of 40% in the tetragonal phase (300 K), in correspondence of the ferroelectric transition. The increase of the magnetic coercive field is strictly related to the re-orientation of ferroelectric domains, which induces a local strain (about 1.25% [44]) in the Fe epitaxial film and hardens the magnetic transition via the creation of stronger pinning sites for the magnetic domain-wall motion.

However, BTO thin films grown on suitable substrates are definitely more interesting in view of integration in practical devices. Recently we have demonstrated [45] that in these systems mechanical clamping from the substrate suppresses the strain-mediated MEC, due to the suppression of BTO tetragons reorientation during FE transitions [46,47]. Moreover, we have shown that, in fully epitaxial Fe/MgO/Fe tunneling junctions grown on BTO, no sizable variations of the magnetic coercive fields or of the tunneling magnetoresistance (TMR) take place upon reversal of the polarization of the BTO layer [45]. We explained this result in terms of the strong localization of MEC at the Fe/BTO interface. As the TMR depends on the Fe density of states at the MgO/Fe interface, that is physically separated from the Fe/BTO interface at which MEC is localized (the thickness of the bottom Fe layer in contact with BTO is 3 nm in Ref. 45), any polarization-dependent magnetic effect is inhibited.

A more promising geometry for exploiting MEC in the Fe/BTO system consists in employing BTO as tunneling barrier in hybrid MFTJs, so that the interfacial Fe layer affected by MEC is the same involved in tunneling, as predicted by first principle calculations on $Fe/BaTiO_3/Fe$ [22] and $SrRuO_3/BaTiO_3/SrRuO_3$ [23]. Recent experiments on MFTJs based on $Fe/BTO/La_{2/3}Sr_{1/3}MnO_3$ (LSMO) heterostructures suggest the existence of pure electronic interfacial MEC mechanisms in these fully-epitaxial systems. Garcia et al. [24] demonstrated the nonvolatile electric control of the tunnel magnetoresistance (TMR) in artificial $Fe/BTO/La_{2/3}Sr_{1/3}MnO_3$ (LSMO) nano-sized tunnel junctions (MFTJs) after switching the electrical polarization of the tunnel barrier, reflecting the modulation of the carriers spin polarization by the direction of FE polarization. In addition, evidence for remanent induced magnetic moments on Ti and O atoms, coupled to those of Fe, was observed in Fe/BTO/LSMO heterostructures by means of X-ray resonant magnetic scattering measurements [25].

More recently we provided [48] a direct experimental proof of the room temperature electrical "on-off" switching of the magnetic ordering within the interfacial Fe layer in contact with BTO in Co/Fe/BTO/LSMO heterostructures. By X-ray magnetic circular dichroism we found that it is possible to create or suppress the ferromagnetic order just within the interfacial oxidized Fe layer by reversing the dielectric polarization of the adjacent BTO. In this paper, we report on the application of such on/off magnetic switching to micron-sized multiferroic tunneling junctions (MFTJ), with ferroelectric barrier (BTO) and ferromagnetic electrodes (Fe and LSMO). In Sec. 2 we discuss the general properties of the Fe/BTO interface and we briefly summarize the results shown in Ref. 48. In Sec. 3 we report on the realization of the Fe/BTO/LSMO heterostructure and the fabrication of the tunneling devices. In Sec. 4 we present the magneto-electrical characterization of the device, demonstrating that electric control of spin polarization and magneto-transport properties can be achieved. In Sec. 5, conclusions and future perspectives of this approach are discussed.

2. The Fe/$BaTiO_3$ interface

Thanks to the small lattice mismatch, high quality epitaxial Fe/BTO interfaces can be synthesized. First BTO films are grown by pulsed laser deposition onto an LSMO/STO template according to an optimized recipe described in ref [49]. The SrTiO3 (STO) substrate has been chosen for different reasons. The lattice mismatch between the in-plane lattice parameters of STO and BTO is 2.3% when bulk values are considered, so that BTO films grow cube on cube on STO(001), with a small in-plane compressive strain which tends to stabilize tetragonality and ferroelectricity [49,50]. Even when a buffer layer of LSMO (as in our case) is inserted in between STO and BTO, the epitaxy is fully preserved, as shown by TEM measurements [48]. Moreover, STO is fully CMOS compatible, because of the possibility of epitaxially growing STO films on Si substrates has been largely demonstrated employing proper buffer layers, prepared by Pulsed Laser Deposition (PLD) [51,52] and/or Molecular Beam Epitaxy (MBE) [53,54,55]. The Fe layer is then epitaxially grown on BTO by molecular beam epitaxy, without breaking vacuum, in such a way to obtain good crystallinity and negligible chemical interdiffusion [56]. For a deposition

temperature of 373 K and a post-annealing treatment at 473 K just an interfacial monolayer of oxidized iron is detected, which appears as an unavoidable consequence of the $Fe/BaTiO_3$ chemical interaction. We employed these high quality samples to investigate the origin of magnetoelectric coupling at the Fe/BTO interface [48].

To this scope we exploited the chemical sensitivity of XMCD to probe the magnetic properties of an ultrathin Fe layer in contact with BTO, as a function of the BTO dielectric polarization, in $Au/Co/Fe/BTO/LSMO/SrTiO_3$ capacitors with 0.02 mm^2 area suitable for easy polarization reversal under the synchrotron radiation beam. The nominal thickness of the Fe film was 2 monolayers (ML), where 1 ML corresponds to the spacing between two adjacent Fe layers in the bcc structure (0.143 nm). The role of the Co layer (1 nm thick) is to stabilize the ferromagnetism of the ultrathin Fe film, that otherwise would display superparamagnetic behavior because of the formation of nano-islands at the early stage of Fe growth on BTO. The Au layer acts as capping layer for preventing Co from oxidation. The BTO (150 nm thick) and LSMO (50 nm thick) layers represent the dielectric and the bottom electrode (the top electrode is the Au/Co/Fe trilayer) of the capacitor, respectively. More details on sample growth and characterization are reported in Ref. 48.

In Figure 1 we present X-ray absorption and magnetic circular dichroism spectra (XAS and XMCD, respectively) of the Fe-$L_{2,3}$ peak, taken at room temperature on the micro-capacitors described above. In panels (a) and (c) are reported the XAS spectra measured after polarization of BTO with +5V (P_{up}, corresponding to an electric field E=+170 kV/cm and a remanent polarization P~+10 $\mu C/cm^2$) and -5V (P_{dn}, corresponding to E=-170 kV/cm and P~-10 $\mu C/cm^2$). The spectra labelled s+ (s-) correspond to the sum of Fe-$L_{2,3}$ spectra collected with (σ^+,m^+) and (σ^-,m^-) ((σ^+,m^-) and (σ^-,m^+)), where σ^+ and σ^- indicate the light helicity and m^+ and m^- the magnetization directions. In the insets visual schemes for the Fe/BTO interface in the two different situations are shown: the vertical arrow indicate the BTO polarization direction, while M and M_{Ox} represent the net magnetization in metallic Fe (Fe^0) and in the Fe oxidized layer (Fe_{Ox}) that develops at the Fe/BTO interface. In panel (b) the XMCD signal, taken from the XAS spectra in panels (a) and (c) in the Fe-L_3 region, is reported. The gray shaded area indicates the

region of the spectra where a shoulder corresponding to the oxidized Fe layer in contact with BTO appears. Noteworthy, this component displays a net XMCD signal only when the BTO polarization points towards the Fe layer (P_{up}), while no signal is present when points in the opposite direction (P_{dn}). These results demonstrate that the oxidized Fe layer undergoes a reversible transition (from a ferromagnetic state for P_{up} to a non-magnetic state for P_{dn}) driven by the switching of the electric state of the FE layer. As a matter of fact, DFT calculations show that the Fe/BTO interface is markedly asymmetric with respect to the BTO polarization. While for P_{up} the oxidized interfacial layer displays a robust ferromagnetic order, for P_{dn} the exchange constants are weakened or even change sign, depending on the strength of electronic correlation, so that the system tends to develop an antiferromagnetic order.

This new physical mechanism provides a record value of interfacial MEC, as the interfacial magnetization can be set or suppressed at will. Even though the effect is strongly confined within the Fe layer in contact with BTO, in a hybrid MTJ with a FE tunneling barrier (MFTJ) this would not be an issue. In fact the TMR is mainly determined by the interfacial effective spin polarization, and that of the Fe interfacial layer is suppressed for P_{dn} , which destroys magnetic order. In these hybrid devices, the dielectric polarization then could determine the overall impedance via two mechanisms: (i) the conventional tunneling electroresistance due to the barrier profile modification induced by polarization reversal, and (ii) the on-off switching of the interfacial magnetization in one of the FM electrodes. The combination of these effects is highly appealing in view of the realization of non-conventional memory devices such as ferroelectric memristors [26].

3. Device fabrication

Hybrid MFTJs have been fabricated using the very same stack employed for XMCD experiments, except for the BTO thickness that has been strongly reduced to allow for tunneling. The Au/Co/Fe/BTO/LSMO heterostructures have been grown by the combined use of Pulsed Laser Deposition (PLD) and Molecular Beam Epitaxy (MBE) in a cluster tool where the two deposition techniques are available in-

situ, together with X-ray Photoemission Spectroscopy (XPS) and Diffraction (XPD) for investigating the chemical and structural properties of the sample, respectively [57]. LSMO has been chosen as bottom electrode because it allows for the epitaxial growth of BTO and it displays half-metallicity at cryogenic temperature, with a spin polarization near unity (95%) at 4 K [58,59]. LSMO films with nominal thickness of 50 nm have been grown onto $SrTiO_3$(001) commercial substrates, according to a growth procedure optimized in order to obtain low roughness (<0.2 nm), as measured by Atomic Force Microscopy (AFM), and good magnetic properties (saturation magnetization of 196±0.5 μemu/cm³ at room temperature and Curie temperature of 321±2 K, as measured by Vibrating Sample Magnetometry). Before the growth, an annealing of the substrate up to 1000 K in a 0.29 mbar oxygen pressure has been performed for cleaning and ordering the surface, with the temperature being controlled by a pyrometer. A quadrupled Q-Switched Nd:YAG laser (266 nm), operating at a repetition frequency of 2 Hz and providing pulses 7 ns long, has been employed to generate a plasma from a LSMO stoichiometric target placed in front of the substrate. The LSMO growth has been performed at 1000 K with a 0.29 mbar oxygen pressure; the laser fluence was 5.2 J/cm^2, resulting in a deposition rate of 1.82±0.2 nm/min as measured by the RHEED oscillation period and by X-Ray Reflectometry (XRR) on test samples. Subsequently, a BTO film with nominal thickness of 2 nm (corresponding to about 5 cells) has been deposited on LSMO, according to a growth procedure optimized in order to obtain BTO layers with low roughness and good ferroelectric properties. The BTO growth has been performed at 913 K with 0.027 mbar oxygen pressure and a laser fluence of 2.2 J/cm^2; the deposition rate was 1.85±0.2 nm/min as measured by the RHEED oscillation period and XRR. After deposition, the sample has been post-annealed in 1 atm of oxygen at 873 K for half an hour and then cooled down to room temperature.

Figure 2a reports an AFM image of the BTO surface, from which a roughness of 0.16 nm can be estimated over a 1x1μm² area, comparable with the roughness of the STO substrate. In Figure 2b a polarization vs. voltage curve of a 150 nm thick BTO film grown is shown, as measured with an excitation signal of amplitude 7 V and frequency 100 Hz (a TF Analyzer 2000 from AixACCT Co. has

been employed), from which a saturation polarization of 10±1 μC/cm² has been inferred. The persistence of ferroelectricity even in ultrathin films employed in MFTJs has been separately confirmed by Piezo-Force Microscopy measurements (data not shown). The Au(10 nm)/Co(1 nm)/Fe(2 ML) overlayer has been grown in ultra-high-vacuum conditions (pressure lower than $1x10^{-9}$ mbar) in a dedicated MBE chamber connected to the PLD system, in order to perform the whole growth process without breaking the vacuum [57]. The thickness of the different layers were calibrated by a quartz microbalance and checked by XPS. Between Fe and Co growths, a 20 minutes post-annealing at 473 K has been performed to improve Fe crystal quality.

In Figure 3a we report the 3D view of an MFTJ device, fabricated by optical lithography, ion milling, e-beam deposition of the metallic contacts (Au/Cr), and magnetron sputtering growth of the SiO_2 insulating layer. The vertical junction is connected in a cross-strip geometry to two top and bottom contact pads, made of Au(300 nm)/Cr(7 nm). Note that bottom contacts are junctions themselves but, thanks to their greater area (0.2 mm^2), their series resistance is negligible with respect to the real junction one, whose area is lower than 1600 μm^2. To ensure proper insulation between top and bottom contacts, a 30 nm thick layer of SiO_2 has been used. Each sample (10x10 mm^2) can arrange up to 36 junctions with different shape and area, ranging from 16 μm^2 to 1600 μm^2. Thanks to the geometry of the device, electrical measurements can be performed both in two- and four-probes geometry. In most of the devices, however, the junction resistance was more than 100 times larger than that of the contacts, so that the two methods give almost identical results.

Measurements were taken both at room temperature and in a helium cooled cryostat. In the first case, a Keithley 236 sourcemeter and a Keithley 182 voltmeter were employed, connected to a mechanical probe station. In the second, junctions were wire bonded to a chip carrier mounted on the cryostat and measured with a Keithley 2611 sourcemeter + voltmeter. In order to investigate the transport regime, the current-voltage $I(V)$ curve of each junction has been measured. In Figure 3b the $I(V)$ characteristic (black squares) and the differential conductance (red dashed line) of a junction with 225 μm^2 area, measured at room temperature, are reported. From now on, a positive (negative) voltage

corresponds to current flowing from top to bottom (from bottom to top) contacts, i.e. from Fe to LSMO (from LSMO to Fe). The characteristics is highly nonlinear and the conductance (d*I*/d*V*) displays a parabolic shape, as expected for tunneling junctions. From the different I(V) curves taken at room temperature, a resistance-area product of $2.6\pm1.2 \times 10^3\ \Omega\ \mu m^2$ has been measured at +100 mV bias on devices with area ranging between 16 μm^2 to 1600 μm^2.

4. Magnetoelectric characterization

Conventional FE measurements, based on the detection of switching current, are prevented on tunneling junctions by the intrinsic parallel conduction channel due to tunneling. For this reason, we used the TER effect to identify the coercive voltages needed to switch the BTO polarization within the barrier. In Figure 4 we report the resistance of a junction with 15x15 μm^2 area, measured at 20K with a bias of 50 mV, while sweeping the voltage of polarization pulses between -1.5 V and + 2V. The two FE switching are clearly seen, leading to distinct states of the tunnel resistance and a TER value, defined as $(R_{dn}-R_{up})/R_{up}$, of $12\pm0.1\%$. Note, however, that the complete FE saturation could not have been reached, as we limited the current below 8×10^3 A/cm^2 to preserve the junction integrity. For magnetoelectric measurements we thus used +2V to induce a BTO remanent polarization pointing out of the Fe layer (P_{dn}) and -1.3 V for the opposite state (P_{up}). The asymmetry between these two values depends on the barrier asymmetry, due to the different interfaces involved (Fe/BTO and BTO/LSMO), but does not affect the results presented below, because in both cases a remanent state in BTO is set. Note also that here the state P_{dn} is obtained for positive bias, while in case of XMCD measurements of Figure 1 it was for negative bias. This is because in XMCD measurements the bias was applied in a top-top configuration, between the top electrode of two adjacent capacitors, with that under measurement by XMCD grounded via the picoammeter and the bias voltage applied to the second one.

In Figure 5 we report the magnetoresistance (*R* vs. *H*) curves, taken on a 15x15 μm^2 junction at 20 K, for the two opposite states of polarization: P_{dn} (+2V) and P_{up} (-1.3V), corresponding to the dielectric

polarization of BTO pointing out of or towards the Fe layer, respectively. After poling the junction in the P_{up} or P_{dn} configurations with 0.5 s long voltage pulses, the voltage is reduced to 80 mV for magnetoresistance measurements, in such a way to get a good signal-to-noise ratio without modifying the polarization configuration of BTO. The magnetic field *H* is applied in plane along the [100] direction of the Fe layer, corresponding to magnetic easy axis.

For both polarizations, the *R* vs. *H* curve displays a butterfly shape, characteristic of tunneling magnetoresistance when the two magnetic layers present different coercive fields but none of them is blocked. We note that, at the maximum field (~300 Oe) we could achieve with the experimental setup, the resistance is not asymptotically saturated but presents a parabolic shape. This is due to the magnetoresistance of the bottom contact of LSMO, that adds up to the tunneling resistance of the device. The minimum value of the resistance is found at an applied magnetic field of 48 Oe, but we do not observe the clear plateau which is the signature of antiparallel alignment between Co/Fe and LSMO. This is likely due to the very similar coercive fields of Co/Fe and LSMO layers, as well as to some coupling between the magnetic layers due to the very low barrier thickness (2 nm). The small values of TMR (-0.32%$\pm$0.05% for P_{up} and -0.12%$\pm$0.05% for P_{dn}), calculated on the curves reported in Figure 5 after background subtraction, can also be explained by the difficulty to achieve the antiparallel configuration in these junctions, which have been fabricated using exactly the same structure used for XMCD experiments, to allow for a direct comparison. Note however that the negative sign of the magnetoresistance (the parallel state is more resistive than the antiparallel one) is in agreement with the pioneering work by Garcia et al. [24] and quite typical for such kind of junctions involving LSMO and 3d metals [60].

We note also that the reduction of TMR absolute value in the P_{dn} state is coherent with the results of XMCD experiments presented above showing the on-off switching of the interface magnetization induced by the FE polarization. The TMR is larger in the P_{up} state, corresponding to the ferromagnetic order of the interfacial Fe layer, than in the P_{dn} state, corresponding to a non magnetic behavior of the interfacial Fe layer. The strong localization of the MEC effects at the Fe/BTO interface can explain the

non complete disappearance of the TMR for P_{dn}. Contributions to tunneling from the second Fe monolayer, whose magnetic order is unaffected by the reversal of the BTO polarization, as well as from Co atoms close to the barrier due to some inhomogeneity of the Fe layer thickness, can largely account for this. Note that, while the on-off switching of the Fe interfacial magnetization survives up to room temperature, the observed TMR decreases quickly while temperature increases. This is essentially due to the temperature dependence of TMR, that completely disappears around 230 K, due to the well known problem of fast decrease of interfacial LSMO spin polarization when approaching room temperature [61].

5. Conclusions

In this paper we reported on a pure electric mechanism for achieving the electrical control of the interfacial spin polarization and magnetoresistance in Au/Co/Fe/BTO/LSMO hybrid ferroelectric magnetic tunneling junctions. We show that, at 20 K, devices with 2 nm BTO barrier present both TER (12$\pm$0.1%) and TMR. Even though the TMR is small (-0.32%$\pm$0.05% for P_{up} and -0.12%$\pm$0.05% for P_{dn}), its dependence on the BTO polarization is clear and consistent with the on-off switching of the Fe magnetization at the Fe/BTO interface found by XMCD. Further improvements of the prototypal device presented in this paper require the optimization of the LSMO magnetic properties or the replacement of this layer, in order to extend the working regime towards room temperature, as well as the achievement of a well-defined antiparallel state which is needed to increase the absolute TMR values.

Acknowledgements

We acknowledge M. Leone for his skillful technical assistance. This work was partially funded by Fondazione Cariplo via the project Magister (Project No. 2013-0726) and by Italian Ministry of Research via the project FIRB OSSIDI NANOSTRUTTURATI: MULTI-FUNZIONALITA' E APPLICAZIONI (RBAP115AYN).

Figures

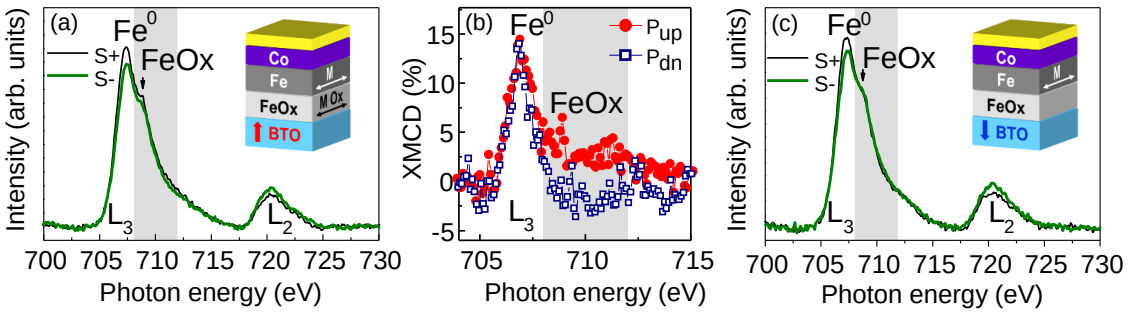

Figure 1: a-c) XAS Fe-L2,3 spectra taken at room temperature on Au/Co/Fe/BTO/LSMO/STO capacitors after polarization of BTO with (a) +5 V (P_{up}) and (b) -5 V (P_{dn}) respectively. Voltages are applied in a top-top configuration, between two adjacent pillars connected through the bottom LSMO layer, while the pillar probed by XMCD was grounded via the pico-ammeter. Insets in (a) and (c) are visual schemes of the Fe/BTO interface for P_{up} and P_{dn}: vertical arrows correspond to BTO polarization direction, while M and MOx indicate the net magnetization in metallic Fe (Fe^0) and in the Fe oxide layer (FeOx) at the Fe/BTO interface. (b) XMCD signal in the Fe-L3 energy region for BTO polarization P_{up} (red full circles) and P_{dn} (blue empty squares). The gray shading indicates the region of the spectra corresponding to the oxidized Fe layer in contact with BTO. (Adapted from G. Radaelli *et al.* 2014 *Nat. Comm.* **5** 3404)

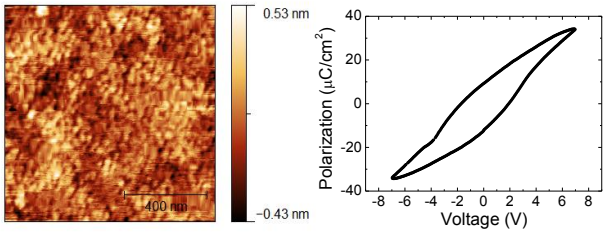

(a) (b)

Figure 2: (a) AFM image and (b) ferroelectric hysteresis loop of a 150 nm-thick BTO test sample, grown on LSMO/STO in the same conditions of the heterostructures employed in magneto-electric measurements, under an excitation signal of frequency 100 Hz. Leakage contribution to the hysteresis cycle is subtracted by software.

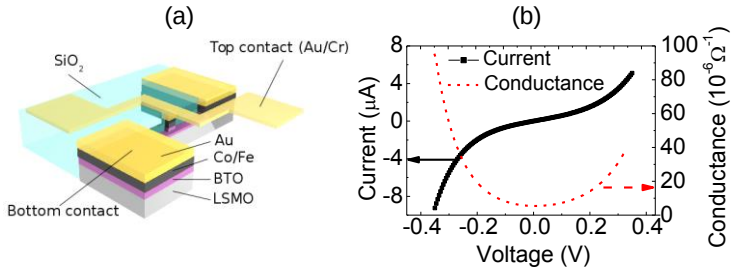

Figure 3: (a) 3D view of the Au/Co/Fe/BTO/LSMO/STO multiferroic tunneling device; (b) current-voltage characteristics (black squares) and differential conductance (red dashed line) of a device with 225 μm^2 area. The parabolic trend of the conductance is a clear signature of the tunneling regime.

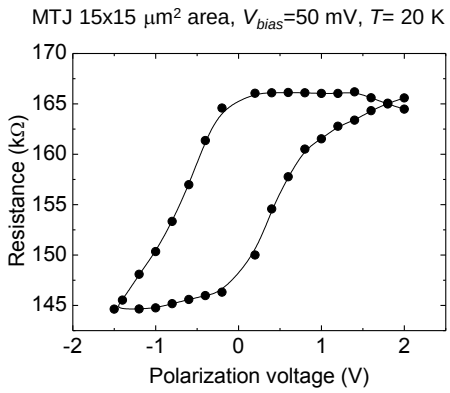

Figure 4: Resistance versus polarization voltage at 20K and 50mV bias, showing a TER of about 12%.

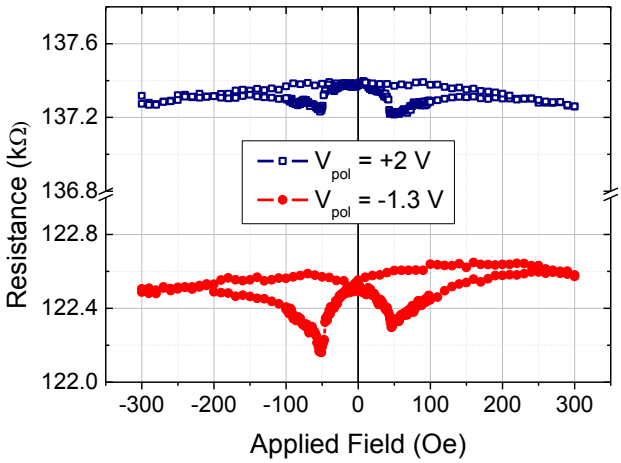

Figure 5: TMR measurements at 20 K and 80 mV bias, after having polarized the BTO with +2 V (P_{dn}, blue curve) and -1.3 V (P_{up}, red curve).

REFERENCES

[1] Cheong S-W and Mostovoy M 2007 Multiferroics: a magnetic twist for ferroelectricity *Nat. Mat.* **6** 13-20

[2] Khomskii D 2009 Classifying multiferroics: Mechanisms and effects *Physics* **2** 20

[3] Khomskii D I 2006 Multiferroics: Different ways to combine magnetism and ferroelectricity *J. Magn. Magn. Mat.* **306** 1-8

[4] Fiebig M 2005 Revival of the magnetoelectric effect *J. Phys. D: Appl. Phys.* **38** R123-R152

[5] Nan C W, Bichurin M I, Dong S, Viehland D and Srinivasan G 2008 Multiferroic magnetoelectric composites: Historical perspective, status, and future directions *J. Appl. Phys.* **103** 031101

[6] Ma J, Hu J, Li Z and Nan C W 2011 Recent progress in multiferroic magnetoelectric composites: From bulk to thin films *Adv. Mater.* **23** 1062–87

[7] Velev J P, Jaswal S S and Tsymbal E Y 2011 Multi-ferroic and magnetoelectric materials and interfaces. *Philos. Trans. A. Math. Phys. Eng. Sci.* **369** 3069–97

[8] Vaz C A F, Hoffman J, Ahn C H, and Ramesh R 2010 Magnetoelectric Coupling Effects in Multiferroic Complex Oxide Composite Structures *Adv. Mat.* **22** 2900-2918

[9] Bibes M 2012 Nanoferronics is a winning combination *Nat. Mat..* **11** 354-357

[10] Zhu J-G 2008 Magnetoresistive Random Access Memory: the path to competitiveness and scalability *Proceedings of the IEEE* **96** 1786-1798

[11] Prejbeanu I L, Kerekes M, Sousa R C, Sibuet H, Redon O, Dieny B, and Nozières J P 2007 Thermally assisted MRAM *Journal of Physics: Condensed Matter* **19**, 165218

[12] Khvalkovskiy A V, Apalkov D, Watts S, Chepulskii R, Beach R S, Ong A, Tang X, Driskill-Smith A, Butler W H, Visscher P B, Lottis D, Chen E, Nikitin V, and Krounbi M 2013 Basic principles of STT-MRAM cell operation in memory arrays *J. Phys. D: Appl. Phys.* **46** 074001

[13] Huai Y, Albert F, Nguyen P, Pakala M, and Valet T 2004 Observation of spin transfer switching in deep submicron-sized and low resistance magnetic tunnel junctions *Appl. Phys. Lett.* **84** 3118

[14] Diao Z, Apalkov D, Pakala M, Ding Y, Panchula A, and Huai Y 2005 Spin transfer switching and spin polarization in magnetic tunnel junctions with MgO and AlO_x barriers *Appl. Phys. Lett.* **87** 232502

[15] Garello K, Miron I M, Avci C O, Freimuth F, Mokrousov Y, Blügel S, Auffret S, Boulle O, Gaudin G, and Gambardella P 2013 Symmetry and magnitude of spin-orbit torques in ferromagnetic heterostructures *Nat. Nanotech.* **8** 587-593

[16] Miron I M, Gaudin G, Auffret S, Rodmacq B, Schuhl A, Pizzini S, Vogel J, and Gambardella P 2010 Current-driven spin torque induced by the Rashba effect in a ferromagnetic metal layer *Nat. Mat.* **9** 230-234

[17] Liu L, Pai C-F, Li Y, Tseng H W, Ralph D C, and Buhrman R A 2012 Spin-torque switching with the giant spin Hall effect of Tantalum *Science* **336** 555-558

[18] Kirilyuk A, Kimel A V, Rasing T 2010 Ultrafast optical manipulation of magnetic order *Rev. Mod. Phys.* **82** 2731

[19] Beaurepaire E, Merle J-C, Daunois A, and Bigot J-Y 1996 Ultrafast spin dynamics in ferromagnetic Nickel *Phys. Rev. Lett.* **76** 4250

[20] Hohlfeld J, Gerrits Th, Bilderbeek M, Rasing T, Awano H, and Ohta N 2001 Fast magnetization reversal of GdFeCo induced by femtosecond laser pulses *Phys. Rev. B* **65** 012413

[21] Savoini M, Piovera C, Rinaldi C, Albisetti E, Petti D, Khorsand A R, Duò L, Dallera C, Cantoni M, Bertacco R, Finazzi M, Carpene E, Kimel A V, Kirilyuk A, and Rasing Th 2014 Bias-controlled ultrafast demagnetization in magnetic tunneling junctions *Phys. Rev. B* **89** 140402(R)

[22] Velev J P, Duan C-G, Belashchenko K D, Jaswal S S and Tsymbal E Y 2008 Effects of ferroelecricity and magnetism on electron and spin transport in Fe/$BaTiO_3$/Fe multiferroic tunnel junctions *J. Appl. Phys.* **103** 07A701

[23] Velev J P, Duan C-G, Burton J D, Smogunov A, Niranjan M K, Tosatti E, Jaswal S S and Tsymbal E Y 2009 Magnetic Tunnel Junctions with Ferroelectric Barriers: Prediction of Four Resistance States from First Principles. *Nano Lett.* **9** 427–32

[24] Garcia V, Bibes M, Bocher L, Valencia S, Kronast F, Crassous A, Moya X, Enouz-Vedrenne S, Gloter A, Imhoff D, Deranlot C, Mathur N D, Fusil S, Bouzehouane K and Barthélémy A 2010 Ferroelectric Control of Spin Polarization. *Science* **327** 1106–10

[25] Valencia S, Crassous A, Bocher L, Garcia V, Moya X, Cherifi R O, Deranlot C, Bouzehouane K, Fusil S, Zobelli A, Gloter A, Mathur N D, Gaupp A, Abrudan R, Radu F, Barthélémy A and Bibes M 2011 Interface-induced room-temperature multiferroicity in BaTiO3. *Nat. Mater.* **10** 753–8

[26] Chanthbouala A, Garcia V, Cherifi R O, Bouzehouane K, Fusil S, Moya X, Xavier S, Yamada H, Deranlot C, Mathur N D, Bibes M, Barthélémy A and Grollier J 2012 A Ferroelectric Memristor. *Nat. Mater.* **11** 860–4

[27] Pantel D, Goetze S, Hesse D and Alexe M 2012 Reversible Electrical Switching of Spin Polarization in Multiferroic Tunnel Junctions. *Nat. Mater.* **11** 289–93

[28] Chanthbouala A, Crassous A, Garcia V, Bouzehouane K, Fusil S, Moya X, Allibe J, Dlubak B, Grollier J, Xavier S, Deranlot C, Moshar A, Proksch R, Mathur N D, Bibes M and Barthélémy A 2012 Solid-state memories based on ferroelectric tunnel junctions. *Nat. Nanotechnol.* **7** 101–4

[29] Yin Y W, Burton J D, Kim Y-M, Borisevich a Y, Pennycook S J, Yang S M, Noh T W, Gruverman a, Li X G, Tsymbal E Y and Li Q 2013 Enhanced tunnelling electroresistance effect due to a ferroelectrically induced phase transition at a magnetic complex oxide interface. *Nat. Mater.* **12** 397–402

[30] Garcia V and Bibes M 2014 Ferroelectric Tunnel Junctions for Information Storage and Processing. *Nat. Commun.* **5** 4289

[31] Zhou Y 2011 Tunneling magnetoresistance modulation in a magnetic tunnel junction with a ferroelectric barrier. *Nanotechnology* **22** 085202

[32] Burton J D and Tsymbal E Y 2011 Giant Tunneling Electroresistance Effect driven by an Electrically Controlled Spin Valve at a Complex Oxide Interface *Phys. Rev. Lett.* **106** 157203

[33] Buzzi M, Chopdekar R V., Hockel J L, Bur a., Wu T, Pilet N, Warnicke P, Carman G P, Heyderman L J and Nolting F 2013 Single domain spin manipulation by electric fields in strain coupled artificial multiferroic nanostructures *Phys. Rev. Lett.* **111** 1–5

[34] Laukhin V, Skumryev V, Martí X, Hrabovsky D, Sánchez F, García-Cuenca M V, Ferrater C, Varela M, Lüders U, Bobo J F, and Fontcuberta J 2006 Electric-Field Control of Exchange Bias in Multiferroic Epitaxial Heterostructures *Phys. Rev. Lett*. **97** 227201

[35] Skumryev V, Laukhin V, Fina I, Martí X, Sánchez F, Gospodinov M, and Fontcuberta J 2011 Magnetization Reversal by Electric-Field Decoupling of Magnetic and Ferroelectric Domain Walls in Multiferroic-Based Heterostructures *Phys. Rev. Lett*. **106** 057206

[36] He X, Wang Y, Wu N, Caruso A N, Vescovo E, Belashchenko K D, Dowben P A, and Binek C 2010 Robust isothermal electric control of exchange bias at room temperature *Nat. Mat.* **9** 579-585

[37] Wu S M, Cybart S A, Yu P, Rossell M D, Zhang J X, Ramesh R, and Dynes R C 2010 Reversible electric control of exchange bias in a multiferroic field-effect device *Nat. Mat.* **9** 756-761

[38] Molegraaf H J A, Hoffman J, Vaz C A F, Gariglio S, van der Marel D, Ahn C H, and Triscone J-M 2009 Magnetoelectric Effects in Complex Oxides with Competing Ground States *Adv. Mat.* **21** 3470-3474

[39] Maruyama T, Shiota Y, Nozaki T, Ohta K, Toda N, Mizuguchi M, Tulapurkar A A, Shinjo T, Shiraishi M, Mizukami S, Ando Y, and Suzuki Y 2009 Large voltage-induced magnetic anisotropy change in a few atomic layers of iron *Nat. Nanotech*. **4** 158-161

[40] Duan C-G, Jaswal S S, and Tsymbal E Y 2006 Predicted magnetoelectric effect in Fe/$BaTiO_3$ multilayers: Ferroelectric control of magnetism *Phys. Rev. Lett*. **97** 047201

[41] Duan C-G, Velev J P, Sabirianov R F, Zhu Z, Chu J, Jaswal S S, and Tsymbal E Y 2008 Surface Magnetoelectric Effect in Ferromagnetic Metal Films *Phys. Rev. Lett.* **101** 137201

[42] Sahoo S, Polisetty S, Duan C-G, Jaswal S S, Tsymbal E Y, and Binek C 2007 Ferroelectric control of magnetism in $BaTiO_3$/Fe heterostructures via interface strain coupling *Phys. Rev. B* **76** 092108

[43] Brivio S, Petti D, Bertacco R, and Cezar J C 2011 Electric field control of magnetic anisotropies and magnetic coercivity in Fe/$BaTiO_3$ (001) heterostructures *Appl. Phys. Lett.* **98** 092505

[44] Geprägs S, Brandlmaier A, Opel M, Gross R, and Goennenwein S T B 2010 Electric field controlled manipulation of the magnetization in Ni/$BaTiO_3$ hybrid structures *Appl. Phys. Lett.* **96** 142509

[45] Radaelli G, Petti D, Cantoni M, Rinaldi C, and Bertacco R 2014 Absence of strain-mediated magnetoelectric coupling at fully epitaxial Fe/$BaTiO_3$ interface *J. Appl. Phys.* **115** 172604

[46] Zheng H, Wang J, Lofland S E, Ma Z, Mohaddes-Ardabili L, Zhao T, Salamanca-Riba L, Shinde S R, Ogale S B, Bai F, Viehland D, Jia Y, Schlom D G, Wuttig M, Roytburd A and Ramesh R 2004 Multiferroic $BaTiO_3$-$CoFe_2O_4$ Nanostructures *Science* **303** 661-663

[47] Schlom D G, Chen L Q, Eom C B, Rabe K M, Streiffer S K, and Triscone J M 2007 Strain tuning of ferroelectric thin films *Annu. Rev. Mater. Res.* **37** 589-626

[48] Radaelli G, Petti D, Plekhanov E, Fina I, Torelli P, Salles B R, Cantoni M, Rinaldi C, Gutiérrez D, Panaccione G, Varela M, Picozzi S, Fontcuberta J, and Bertacco R 2014 Electric control of ferromagnetic order at the Fe/$BaTiO_3$ interface *Nat. Comm.* **5**, 3404

[49] Radaelli G, Brivio S, Fina I and Bertacco R 2012 Correlation between Growth Dynamics and Dielectric Properties of Epitaxial BaTiO3 Films *Appl. Phys. Lett.* **100** 102904

[50] Brivio S, Rinaldi C, Petti D, Bertacco R, and Sanchez F 2010 Epitaxial growth of Fe/$BaTiO_3$ heterostructures *Thin Solid Films* **519** 5804

[51] Scigaj M, Dix N, Fina I, Bachelet R, Warot-Fonrose B, Fontcuberta J, and Sanchez F 2013 Ultra-flat $BaTiO_3$ epitaxial films on Si(001) with large out-of-plane polarization *Appl Phys. Lett.* **102** 112905

[52] Singamaneni S R, Fan W, Prater J T, and Narayan J 2014 Magnetic properties of $BaTiO_3/La_{0.7}Sr_{0.3}MnO_3$ thin films integrated on Si(100) *J. Appl. Phys.* **116** 224104

[53] Marchiori C, Sousa M, Guiller A, Siegwart H, Locquet J-P, Fomperyne J, Norga C J, and Seo J W 2006 Thermal stability of the $SrTiO_3$/(Ba,Sr)O stacks epitaxially grown on Si *Appl. Phys. Lett.* **88** 072913

[54] Xiong C, Pernice W H P, Ngai J H, Reiner J W, Kumah D, Walker F J, Ahn C H, and Tang H X 2014 Active silicon integrated nanophotonics: ferroelectric $BaTiO_3$ devices *Nanoletters* **14** 1419-1425

[55] Dubourdieu C, Bruley J, Arruda T M, Posadas A, Jordan-Sweet J, Franck M M, Cartier E, Frank D J, Kalinin S V, Demkov A A, and Narayanan V 2013 Switching of ferroelectric polarization in epitaxial $BaTiO_3$ films on silicon without a conducting bottom electrode *Nat. Nanotech.* **8** 748-754

[56] Radaelli G, Cantoni M, Lijun L, Espahbodi M, and Bertacco R 2014 Two dimensional growth of ultrathin Fe films on $BaTiO_3$ with sharp chemical interface *J. Appl. Phys.* **115** 063501

[57] Bertacco R, Cantoni M, Riva M, Tagliaferri A, and Ciccacci F 2005 Epitaxial growth and characterization of layered magnetic nanostructures *Appl. Surf. Sci.* **252** 1754

[58] Bowen M, Bibes M and Barthélémy A 2003 Nearly Total Spin Polarization in La2/3Sr1/3MnO3 from Tunneling Experiments *Appl. Phys. Lett.* **82** 233

[59] Bowen M, Barthélémy A, Bibes M, Jacquet E, Contour J-P, Fert A, Ciccacci F, Duò L, and Bertacco R 2005 Spin-polarised tunneling spectroscopy in tunnel junctions with half-metallic electrodes *Phys. Rev. Lett.* **95** 137203

[60] De Teresa J M, Barthélémy A, Fert A, Contour J P, Lyonnet R, Montaigne F, Seneor P, and Vaurès A 1999 Inverse tunnel magnetoresistance in Co/$SrTiO_3$/$La_{0.7}Sr_{0.3}MnO_3$: new ideas on spin-polarized tunneling *Phys. Rev. Lett.* **82** 4288-4291

[61] Bertacco R, Tagliaferri A, Riva M, Signorini L, Cantoni M, Cattoni A, Ciccacci F, Davidson B A, Maccherozzi F, Vobornik I, and Panaccione G 2008 Surface electronic and magnetic properties of $La_{2/3}Sr_{1/3}MnO_3$ thin films with extended metallicity above the Curie temperature *Phys. Rev. B* **78** 035448